ARTICLES

Synthesis and Characterization of the $Mg_2Si_xGe_{1-x}$ Solid Solution

Eva Ratai, Matthew P. Augustine,* and Susan M. Kauzlarich*

Department of Chemistry, University of California, One Shields Avenue, Davis, California 95616

Received: February 26, 2003

The $Mg_2Si_xGe_{1-x}$ solid solution was prepared by heating stoichiometric amounts of elemental Mg, Si, and Ge in an argon atmosphere. Both microprobe and X-ray diffraction analysis of the reaction products suggest that homogeneous alloys can be made by heating the elements to 1200 °C, a temperature roughly 100 °C in excess of the melting temperatures for pure Mg_2Si and Mg_2Ge. ^{29}Si solid-state nuclear magnetic resonance was used to characterize the $Mg_2Si_xGe_{1-x}$ solid solution. The ^{29}Si isotropic chemical shift changes consistent with the band gap in these materials while the line width increases with local disorder.

Introduction

Magnesium silicide (Mg_2Si) and magnesium germanide (Mg_2Ge) are intermetallic compounds that crystallize in the antifluorite structure type, a structure with Si in face centered cubic sites and Mg in tetrahedral sites. The antifluorite structure shown in Figure 1 can be described as a Zintl compound where the electropositive Mg metal loses electrons and the electronegative Si or Ge nonmetal formally gains four electrons, as necessary to achieve a filled valence. However, this simplistic view of the chemical bonding in Mg_2Si and Mg_2Ge is not an accurate picture of the true electronic structure. In fact, the limited 8% charge transfer between Mg and Si as measured by X-ray photoelectron spectroscopy suggests that the bonding in Mg_2Si is highly covalent,[1] consistent with theoretical calculations dating back to the early 1960s.[2,3−6] These theoretical efforts have since indicated that both Mg_2Si and Mg_2Ge are direct gap semiconductors.[7−10] These compounds have been considered as anode materials for lithium secondary batteries[13] and as starting materials for silicon and germanium nanoparticles.[15] In addition, the high melting temperature[11,12] and superior thermoelectric properties of these compounds make them promising candidates for lightweight materials in medium to high-temperature applications and semiconductor alloys with energy conversion device applications.[16,17]

An exceptionally useful tool that has been used to characterize a number of transition metal silicides is solid-state nuclear magnetic resonance (NMR) spectroscopy. Here the ^{29}Si chemical shift range relative to the tetramethylsilane (TMS) reference at 0 ppm spans ≈600 ppm. The source of this large chemical shift range is the Knight shift commonly observed in metallic materials or equivalently the paramagnetic contribution to the chemical shift mediated by electron−nucleus contact interactions. It is this mechanism that provides information about characteristics of the conduction band at the silicon site in transition metal silicides via measurement of the anisotropy and asymmetry of the chemical shielding tensor in addition to the isotropic chemical shift. As an example, the ^{29}Si magic angle spinning (MAS) NMR spectrum of NaSi shows fairly diamagnetic shifts of −361 and −365 ppm with respect to TMS resulting from the donation of electrons from the electropositive Na to the electronegative Si.[20] This is in contrast to similar measurements in clathrates where severe paramagnetic shifts are observed.[21−24] This paper presents the NMR characterization of the $Mg_2Si_{1-x}Ge_x$ solid solution for the first time and discusses the relationship of these measurements to the electronic structure of these new mixed materials.

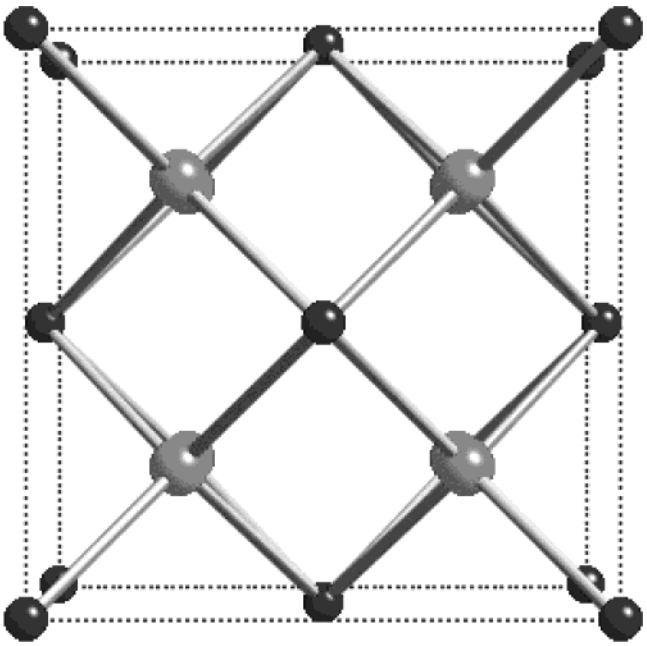

Figure 1. Unit cell of Mg_2Si. It is a face centered (*Fm*3*m*) lattice, which is symmetrically intermeshed with a simple cubic lattice of Mg atoms such that each Mg (large gray circles) is coordinated by four Si atoms in a regular tetrahedron, while each Si (small black circles) is surrounded by a regular cube of eight Mg atoms.

* To whom correspondence should be addressed. E-mail: augustin@chem.ucdavis.edu (M.P.A.); smkauzlarich@ucdavis.edu (S.M.K.).

10.1021/jp030252x CCC: $25.00
Published on Web 10/25/2003

TABLE 1: Microprobe Data for the Solid Solution $Mg_2Si_{1-x}Ge_x$

	weight			chemical analysis		
	atom% Mg	atom% Si	atom% Ge	atom% Mg	atom% Si	atom% Ge
$Mg_2Si_{0.1}Ge_{0.9}$	66.7	3.3	30.0	70.5 ± 0.3	2.5 ± 0.1	27.0 ± 0.3
$Mg_2Si_{0.3}Ge_{0.7}$	66.7	10.0	23.3	70.9 ± 0.7	7.8 ± 0.8	21.3 ± 0.9
$Mg_2Si_{0.4}Ge_{0.6}$	66.7	13.3	20.0	69.9 ± 0.9	12.8 ± 1.0	17.3 ± 0.8
$Mg_2Si_{0.7}Ge_{0.3}$	66.7	23.3	10.0	69.7 ± 1.0	20.9 ± 0.9	9.4 ± 0.6
$Mg_2Si_{0.8}$ $Ge_{0.2}$	66.7	26.7	6.7	69.9 ± 1.3	24.1 ± 1.6	6.0 ± 0.2
Mg_2Si	66.7	33.3	0	68.1 ± 1.0	31.9 ± 1.0	

Experimental Section

Synthesis. Mg_2Si was prepared from stoichiometric amounts of magnesium (99.98%; Johnson Matthey) and silicon (99.9999+%; Johnson Matthey) in tantalum ampules. The ampules (diameter = 10 mm; length ≈60 mm) were etched with an acid solution (20% HF, 25% HNO_3, 55% H_2SO_4) and then crimped and arc welded on one end under an argon atmosphere. Stoichiometric amounts of Mg, Si, and Ge were transferred into the tantalum tube and welded shut in a nitrogen filled drybox. The tantalum tube was sealed into a fused quartz jacket under a reduced pressure of ≈0.2 atm of argon and then heated at a rate of 60 °C/h to 700 °C for 3 days followed by cooling to room temperature at a rate of 30 °C/h. The products were recovered by opening the tubes in a nitrogen filled drybox. Inhomogeneous $Mg_2Si_xGe_{1-x}$ alloys were prepared by the same method as the Mg_2Si compound with the addition of germanium (99.99% Acros) at heating temperatures between 700 and 900 °C. Homogeneous $Mg_2Si_xGe_{1-x}$ alloys were obtained by annealing these inhomogeneous samples to 1200 °C for 8 h.

Microprobe Analysis. Chemical analysis of the $Mg_2Si_xGe_{1-x}$ alloys was performed with a Cameca SX-50 wavelength dispersive electron microprobe operating at an accelerating potential of 20 keV and beam current of 10 nA. Concentrations of Mg, Si, and Ge were determined after applying standard ZAF matrix corrections to the raw data. Net elemental intensities for the alloys were determined from these data with respect to pure elemental calibration standards.

X-ray Powder Diffraction. X-ray powder diffraction data were collected with an INEL CPS 120, which performs the simultaneous collection of 2θ diffracted X-rays over 120°. X-rays (Cu $K\alpha_1$ radiation) were generated with an XRG 3000 source operating at 30 kV and 30 mA. Data acquisition was performed with WinAcq software and was analyzed with MDI Jade. The reflections could be assigned to lattice planes in the Mg_2Si/Mg_2Ge structure. The lattice parameter was determined by a Rietveld refinement program available within the commercial software package (MDI Jade), whereas the silicon-to-germanium ratios were varied according to their composition. The peak profile for all phases was chosen to be a Pearson VII shape and the background was fit with a third-order polynomial. Atomic positions as well as the overall temperature factor were held constant.

Solid-State NMR. All NMR spectra were recorded on a Chemagnetics CMX-400 spectrometer equipped with a Chemagnetics MAS probe configured for O-ring equipped 7.5 mm outer diameter zirconium oxide rotors. The rotors were packed inside of a nitrogen drybox to avoid oxygen contamination. ^{29}Si MAS NMR spectra were obtained at a Larmor frequency of 79.49 MHz and all spectra were acquired with a pulse length of 4 μs (45° tip angle) and a recycle delay of 300 s as the ^{29}Si relaxation time of Mg_2Si is about 600 s. All experiments used MAS speeds of 5 kHz and chemical shifts were externally referenced to TMS.

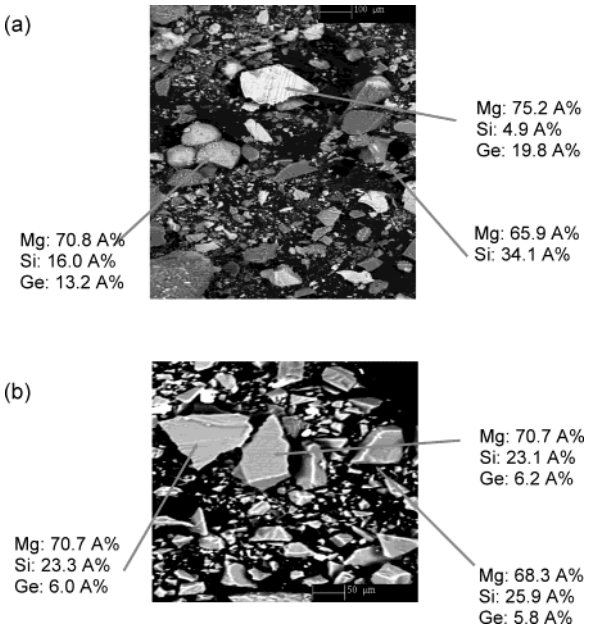

Figure 2. (a) BSE image of $Mg_2Si_{0.3}Ge_{0.7}$ prepared at 900 °C with theoretical amounts of 66.7 atom% Mg, 23.3 atom% Si, 10.0 atom% Ge and the chemical composition obtained by X-ray diffraction for three grains. The different grains show various compositions. (b) BSE image of $Mg_2Si_{0.8}Ge_{0.2}$ reheated at 1200 °C. The different grains exhibit similar composition.

Results

Examples of typical microprobe backscattered electron (BSE) images for the $Mg_2Si_xGe_{1-x}$ alloys prepared in this study are shown in Figure 2. Areas that appear brighter in the image consist of higher atomic number elements. The BSE image shown in Figure 2a for the $Mg_2Si_{0.7}Ge_{0.3}$ alloy prepared at 900 °C illustrates the sample inhomogeneity present prior to sample annealing. Following heating to 1200 °C the BSE image shown in Figure 2b for $Mg_2Si_{0.8}Ge_{0.2}$ becomes uniform suggesting increased sample homogeneity. A summary of this microprobe data yielding alloy composition in Atom% Mg, Si, and Ge and a comparison to similar values obtained by elemental analysis is provided in Table 1.

Figure 3 compares the X-ray diffraction data obtained for Mg_2Si, Mg_2Ge, and the $Mg_2Si_{0.3}Ge_{0.7}$ alloy in parts a−c, respectively. The difference between the measured spectrum shown as the top line and calculation is shown as the lower dispersive like line in each spectrum. Assignment of these data followed by Reitveld refinement resulted in determination of the lattice parameter a as summarized in Table 2.

The ^{29}Si MAS NMR spectrum for Mg_2Si is shown as the lower spectrum in Figure 4. The single 90 Hz (fwhm) resonance at −177.2 ppm is consistent with one crystallographic Si in Mg_2Si. The upper ^{29}Si MAS NMR spectra in Figure 4 show how the ^{29}Si isotropic chemical shift changes with germanium content.

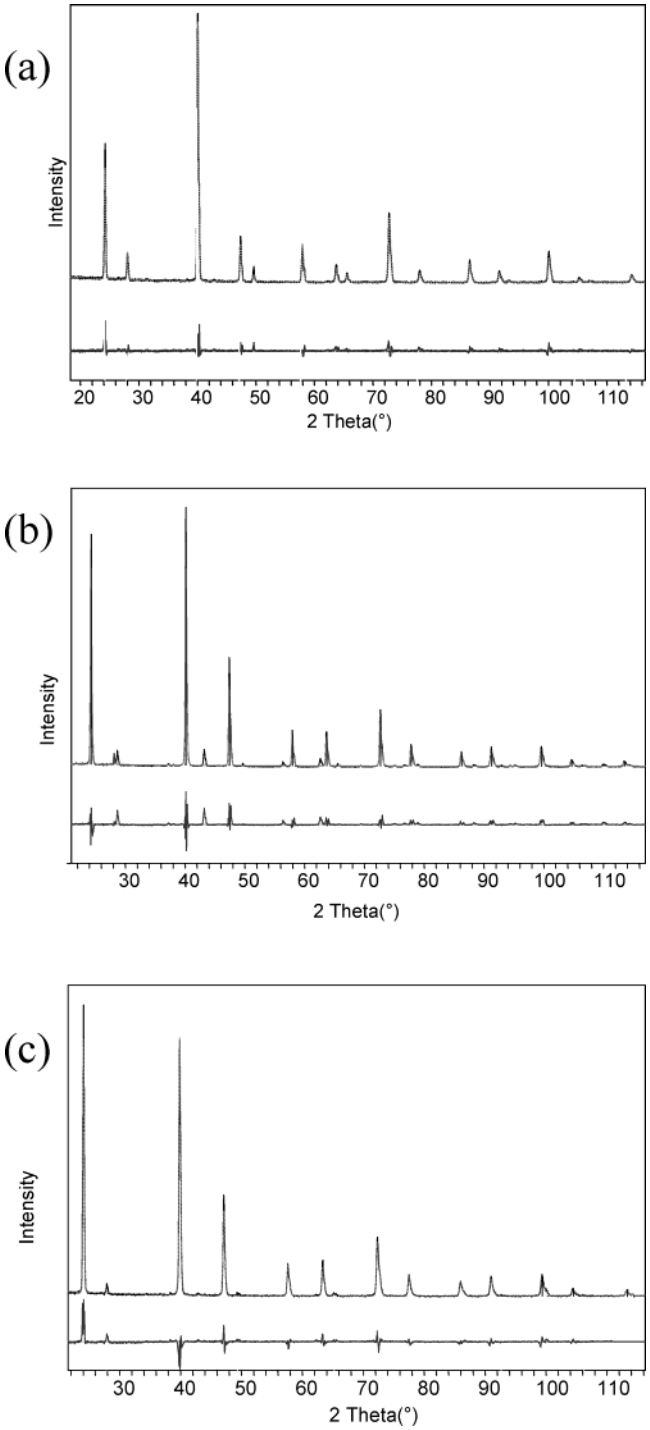

Figure 3. X-ray powder diffraction patterns of (a) Mg_2Si, (b) Mg_2Ge, and (c) $Mg_2Si_{0.3}Ge_{0.7}$ shown in the top line and the differences with calculation shown in the bottom line.

Discussion

Prior to performing any spectroscopic measurements, substantial effort was made to confirm the identity, morphology, and homogeneity of the prepared $Mg_2Si_xGe_{1-x}$ alloys. A combination of the microprobe analysis with the X-ray diffraction data shown in Figures 2 and 3 provided this information. All $Mg_2Si_xGe_{1-x}$ alloys prepared at temperatures between 700 and 900 °C produced BSE images such as the one shown in Figure 2a for $Mg_2Si_{0.7}Ge_{0.3}$ and gave complicated diffraction patterns. Closer inspection of the BSE images revealed substantial grain-to-grain elemental composition heterogeneity as shown by the several gray scale levels represented in Figure 2a. As a point of reference, the elemental content of three separate grains is also shown in Figure 2a. Homogeneous $Mg_2Si_xGe_{1-x}$ alloys were produced by further annealing the samples to 1200 °C for 8 h. By heating the mixture to 1200, 130, and 100 °C above the melting temperatures for Mg_2Si and Mg_2Ge respectively, grain inhomogeneities are removed and uniform samples are produced. The BSE image shown in Figure 2b for the $Mg_2Si_{0.8}Ge_{0.2}$ alloy with limited gray scale levels demonstrates how well the annealing process transforms the heterogeneous alloy into a clean uniform solid solution. Indeed, the ≈11% deviation in Mg content for the three grains shown in Figure 2a is virtually eliminated by annealing where only ≈3% Mg content variation is observed for three randomly chosen particles from Figure 2b. The purity of the annealed $Mg_2Si_xGe_{1-x}$ alloy is born out in the X-ray diffraction data shown in Figure 3c for $x = 0.3$. Comparison of these data to Figure 3, parts a and b, for Mg_2Si and Mg_2Ge, respectively, confirm the presence of a homogeneous mixed solid solution.

Although ^{25}Mg MAS NMR spectra have been previously reported for Mg_2Si, the spectrum shown on the top of Figure 4 is the first ^{29}Si NMR spectrum for this material.[25] The ^{29}Si chemical shift of −177.2 ppm suggests covalent Si−Mg bonding, in contrast to other Si containing Zintl salts such as NaSi. The lack of sidebands in all of the NMR spectra shown in Figure 4 at the modest 5 kHz spinning speed further suggests that the Si site in Mg_2Si and the various alloys is highly

TABLE 2: Results for the X-ray Powder Diffraction Data for $Mg_2Si_{1-x}Ge_x$ Using Rietveld Refinement

	site occupancy			lattice parameter/ Å	sample displacement/ cos θ	R^a/%	E^b/%
	Mg	Si	Ge				
Mg_2Ge	1	0	1	6.3910(4)	0.8	18.1	9.5
$Mg_2Si_{0.1}Ge_{0.9}$	1	0.1	0.9	6.3847(6)	0.7	28.5	5.5
$Mg_2Si_{0.3}Ge_{0.7}$	1	0.3	0.7	6.3837(6)	−0.9	20.4	9.5
$Mg_2Si_{0.4}Ge_{0.6}$	1	0.3	0.6	6.3737(5)	−0.03	14.1	6.1
$Mg_2Si_{0.6}Ge_{0.4}$	1	0.4	0.4	6.3686(1)	0.02	24.2	12.9
$Mg_2Si_{0.7}Ge_{0.3}$	1	0.7	0.3	6.3684(3)	−0.8	17.7	4.2
$Mg_2Si_{0.8}Ge_{0.2}$	1	0.8	0.2	6.3630(3)	−0.08	17.6	8.6
Mg_2Si	1	1	0	6.3524(4)	−0.03	16.5	6.1

[a] $R = 100(\{\sum w(i)[I(0,i) - I(c,i)]^2\}/\{\sum w(i)[I(0,i) - I(b,i)]^2\})^{1/2}$ where $w(i)$ is the statistical weight of the data point i, $I(0,i)$ is the observed intensity of the data point, $I(c,i)$ is the calculated intensity, and $I(b,i)$ is the background intensity. [b] $E = 100[(N - P)/(\sum I(0,i))]^{1/2}$ where N is the number of fitted data points, P is the number of refined parameters, and the sum is over all of the fitted datapoints N that are two standard deviations above the fitted background.

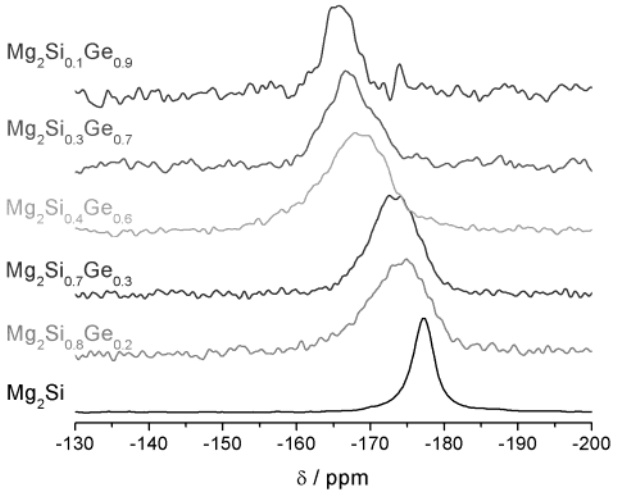

Figure 4. ^{29}Si MAS NMR data as a function of increasing Ge content from bottom to top.

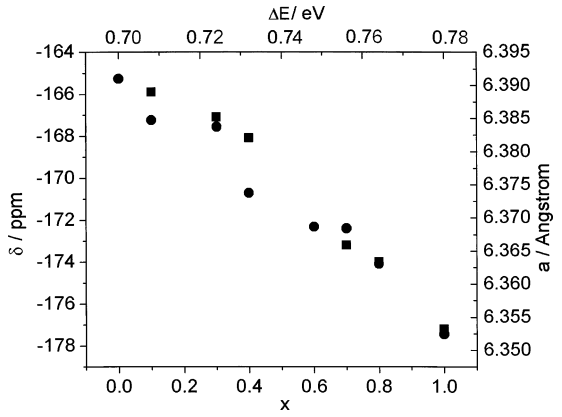

Figure 5. Plot comparing the ^{29}Si chemical shift as solid squares and the lattice parameter as solid circles as a function of both composition x and band gap.

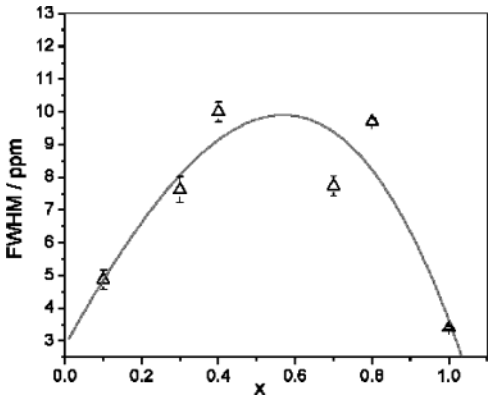

Figure 6. Plot of the full width at half-maximum of the ^{29}Si MAS NMR peak as a function of Ge content $1 - x$. The solid line serves solely as a guide.

symmetric. Again this observation is in contrast with previous ^{29}Si MAS NMR measurements on the Zintl compound NaSi where two resonances centered at -361.2 and -365.5 ppm were observed with large chemical shift anisotropies of $\Delta\delta = 214$ and 236 ppm, respectively. NaSi is a model Zintl phase composed of Si_4^{4-} tetrahedra. The anionic nature of the Si_4^{4-} tetrahedra suggest more electron localization at the Si site yielding a diamagnetic chemical shift in comparison to the primarily covalent bonding network anticipated for the Si sites in Mg_2Si. Here electrons are shared between Mg and Si in the Mg−Si bond thus producing a paramagnetic contribution to the chemical shift.

The trend of the ^{29}Si chemical shift as a function of composition in the annealed $Mg_2Si_xGe_{1-x}$ alloys shown in Figure 4 suggests that Si and Ge atoms are randomly mixed within the crystal structure rather than phase separated. The NMR spectra for the phase separated alloys obtained prior to annealing contained broad featureless lines and displayed little or no variation with composition. This observation is to be expected as each heterogeneous sample contained all possible Si environments that would be expected as a function of composition x. Upon annealing specific Si environments are produced as a function of x and narrow ^{29}Si MAS NMR spectra are observed.

An important comparison between ^{29}Si chemical shift, lattice parameter, and band gap as a function of composition x is shown in Figure 5. Here the black squares correspond to the ^{29}Si chemical shift labeled on the left ordinate as a function of chemical composition x and band gap shown on the lower and upper abscissa, respectively. The black circles track the lattice parameter labeled on the right ordinate as a function of the same abscissa values. The linear variation of lattice parameter with sample composition shown in Figure 5 as the black circles and listed explicitly in Table 2 suggests the presence of a homogeneous solid solution. This X-ray diffraction measurement is in direct agreement with the microprobe data for these compounds, an example of which is shown in Figure 2b.

The variation of the ^{29}Si isotropic chemical shift as a function of band gap is anticipated from the formal theory of chemical shifts. The chemical shift is displayed in all atomic, molecular, and ionic species and describes how electron density shields an applied static magnetic field from a nuclear spin. The shift σ is typically separated into diamagnetic σ_{dia} and paramagnetic σ_{para} parts as $\sigma = \sigma_{dia} + \sigma_{para}$. The diamagnetic part of the chemical shift σ_{dia} is primarily due to electrons occupying orbitals with atomic character. These relatively localized and unperturbed states do not produce a chemical shielding that appreciably varies from compound to compound. The paramagnetic shift σ_{para} on the other hand is an extremely strong function of chemical structure. The source of this shift is a mixing of excited molecular states into the ground state caused by the application of a static magnetic field. This contribution to the overall chemical shift is most sensitive to molecular bonding via the inverse dependence on energy level separation ΔE as

$$\sigma_{para} = -\frac{\mu_0 e^2 \hbar^2}{6\pi m^2} \frac{1}{\Delta E} \left\langle \frac{1}{r^3} \right\rangle \qquad (1)$$

In the special case of a semiconductor, ΔE pertains to the band gap energy, e is the fundamental charge, $\hbar$ is Planck's constant, μ_0 is the vacuum permeability, m is the electron mass, and r is the mean electron-nucleus separation. Returning to Figure 5, the solid line corresponds to a linear regression of the ^{29}Si chemical shift to $1/\Delta E$. The quality of this fit is reliable judging from the r factor value of 0.987. The intercept in this case corresponds to the difference between the reference and diamagnetic shift as $\sigma_{ref} - \sigma_{dia} = (9 \pm 0.7) \times 10^{-5}$ ppm because all ^{29}Si chemical shifts have been externally reference to TMS. The -191 ± 10 ppm eV slope corresponds to $(3.1 \pm 0.2) \times 10^{-23}$ J which can be used along with eq 1 to find the root mean cube distance between the electron and nucleus of 0.91 ± 0.02 Å. Comparison of this distance to the values shown in Table 2 reveal that the electron−nuclear distance is about an order of magnitude less than the value for the lattice parameter a. This result is to be expected given the covalent nature of the bonding in these alloys.

The ^{29}Si NMR data shown in Figure 4 can also provide information regarding alloy heterogeneity from the line width. A summary of these line widths obtained by fitting each of the ^{29}Si NMR spectra in Figure 4 to a Gaussian is shown in Figure 6 as a function of increasing Ge content $1 - x$. As mentioned above, the position of the ^{29}Si NMR peak is a function of electronic structure. The width of the ^{29}Si MAS NMR peak in the solid state where $T_1 \sim T_2 = 600$ s is therefore due to small subtle site-to-site variations in the electronic structure due to the distribution of bond angles and distances between a Si site and its neighbors in the $Mg_2Si_xGe_{1-x}$ solid solution. Indeed the most "ordered" materials Mg_2Si and $Mg_2Si_{0.1}Ge_{0.9}$ display the narrowest lines while the $Mg_2Si_{0.4}Ge_{0.6}$ compound yields the broadest line. In the case of Mg_2Si, a given Si site is surrounded by 12 Si atoms at a distance of 4.4918(3) Å, whereas for pure Mg_2Ge, the Ge site is surrounded by 12 Ge atoms at a distance of 4.5191(3) Å. The preparation of the $Mg_2Si_xGe_{1-x}$ solid solution endeavors to randomly replace the 12 satellite Si atoms

in Mg_2Si with Ge, an action that introduces disorder into a given Si site and ultimately leads to a broad NMR line. The broadest ^{29}Si NMR line is therefore expected to be for $x = 0.5$, consistent with experiment as shown in Figure 6.

Conclusion

The $Mg_2Si_xGe_{1-x}$ solid solution was prepared by heating elemental Mg, Si, and Ge in stoichiometric amounts to 1200 °C. A combination of microprobe analysis with X-ray diffraction suggests that these alloys are homogeneous. ^{29}Si solid state NMR data for these alloys is completely consistent with the microprobe and X-ray data. The band gap dependence of the ^{29}Si chemical shift as a function of Ge content $1 - x$ was used to obtain details about electron-nucleus interactions in the solid solution. Finally, the ^{29}Si NMR line width tracks with the local disorder anticipated for these materials.

Acknowledgment. This work was supported by the Petroleum Research Foundation administered by the American Chemical Society and the National Science Foundation through Grant Nos. DMR-9803074 and 0120990. We thank Shawna Brown and Katherine Pettigrew for aid in sample preparation, Sarah Roeske and Peter Schiffman from the Department of Geology, UC Davis, for the microprobe analysis, John Neil for his help with the Rietveld refinement, and Ping Yu for the use of the W.M. Keck Solid State NMR facility. M.P.A. is a David and Lucile Packard and Alfred P. Sloan Foundation fellow.

References and Notes

(1) van Buuren, M. R. J.; Voermans, F.; van Kempen, H. *J. Phys. Chem.* **1995**, *99*, 9519.
(2) Whitten, W. B.; Chung, P. L.; Danielson, C. *J. Phys. Chem. Solids* **1965**, *26*, 49.
(3) Scouler, W. J. *Phys. Rev.* **1969**, *178*, 1353.
(4) Vazquez, F.; Forman, R. A.; Cardona, M. *Phys. Rev.* **1968**, *176*, 905.
(5) Au-Yang, Y.; Cohen, M. L. *Phys. Rev.* **1969**, *178*, 1358.
(6) Lee, P. M. *Phys. Rev.* **1964**, *135*, A1110.
(7) Wood, D. M.; Zunger, A. *Phys. Rev. B* **1986**, *34*, 4105.
(8) Arnaud, B.; Alouani, M. *Phys. Rev. B* **2000**, *62*, 4464.
(9) Arnaud, B.; Alouani, M. *Phys. Rev. B* **2001**, *64*, 033202.
(10) Krivosheeva, A. V.; Kholod, A. N.; Shaposhnikov, V. L.; Krivosheev, A. E.; Borisenko, V. E. *Semiconductors* **2002**, *36*, 496.
(11) Li, G. H.; Kong, Q. P. *Scr. Metall. Mater. (USA)* **1995**, *32*, 1435.
(12) Li, G. H.; Gill, H. S.; Varin, R. A. *Metall. Trans. A* **1993**, *24A*, 2383.
(13) Moriga, T.; Watanabe, K.; Tsuji, D.; Massaki, S.; Nakabayashi, I. *J. Sol. State Chem.* **2000**, *153*, 386.
(14) Nartowski, A. M.; Parkin, I. P. *Polyhedron* **2002**, *21*, 187.
(15) Yang, C. S.; Bley, R. A.; Kauzlarich, S. M.; Lee, H. W. H.; Delgado, G. R. *J. Am. Chem. Soc.* **1999**, *121*, 5191.
(16) Riffel, M.; Schilz, J. *Scr. Metall. Mater. (USA)* **1995**, *32*, 1951.
(17) Zhang, L. M.; Leng, Y. G.; Jiang, H. Y.; Chen, L. D.; Hirai, T. *Mater. Sci. Eng. B-Solid State Mater.* **2001**, *86*, 195.
(18) LaBotz, R. J.; Mason, D. R. *J. Electrochem. Soc.* **1963**, *110*, 121.
(19) Duncan, T. M.; Hamilton, D. M. *J. Mater. Res. (USA)* **1988**, *3*, 943.
(20) Mayeri, D.; Phillips, B. L.; Augustine, M. P.; Kauzlarich, S. M. *Chem. Mater.* **2001**, *13*, 765.
(21) Gryko, J.; McMillan, P. F.; Sankey, O. F. *Phys. Rev. B-Condensed Matter* **1996**, *54*, 3037.
(22) Ramachandran, G. K.; McMillan, P. F.; Diefenbacher, J.; Gryko, J.; Dong, J. J.; Sankey, O. F., *Phys. Rev. B-Condensed Matter* **1999**, *60*, 12294.
(23) Ramachandran, G. K.; Dong, J. J.; Sankey, O. F.; McMillan, P. F. *Phys. Rev. B* **2001**, *6303*, 3102.
(24) Shimizu, F.; Maniwa, Y.; Kume, K.; Kawaji, H.; Yamanaka, S.; Ishikawa, M. *Synth. Met.* **1997**, *86*, 2141.
(25) Dupree, R.; Smith, M. E. *J. Chem. Soc., Chem. Commun.* **1988**, 1483.